



The Trithorax group protein dMLL3/4 instructs the assembly of the zygotic genome at fertilization

Pedro Prudêncio^{1,2}, Leonardo G Guilgur³, João Sobral³, Jörg D Becker³, Rui Gonçalo Martinho^{1,2,4,*}  & Paulo Navarro-Costa^{1,3,**} 

Abstract

The transition from fertilized oocyte to totipotent embryo relies on maternal factors that are synthesized and accumulated during oocyte development. Yet, it is unclear how oocytes regulate the expression of maternal genes within the transcriptional program of oogenesis. Here, we report that the *Drosophila* Trithorax group protein dMLL3/4 (also known as Trr) is essential for the transition to embryo fate at fertilization. In the absence of dMLL3/4, oocytes develop normally but fail to initiate the embryo mitotic divisions after fertilization. This incapability results from defects in paternal genome reprogramming and maternal meiotic completion. The methyltransferase activity of dMLL3/4 is dispensable for both these processes. We further show that dMLL3/4 promotes the expression of a functionally coherent gene subset that is required for the initiation of post-fertilization development. Accordingly, we identify the evolutionarily conserved IDGF4 glycoprotein (known as oviductin in mammals) as a new oocyte-to-embryo transition gene under direct dMLL3/4 transcriptional control. Based on these observations, we propose that dMLL3/4 plays an instructive role in the oocyte-to-embryo transition that is functionally uncoupled from the requirements of oogenesis.

Keywords chromatin; *Drosophila*; fertilization; Trithorax; zygote

Subject Categories Chromatin, Epigenetics, Genomics & Functional Genomics; Development & Differentiation

DOI 10.15252/embr.201845728 | Received 6 January 2018 | Revised 27 June 2018 | Accepted 2 July 2018 | Published online 23 July 2018

EMBO Reports (2018) 19: e45728

Introduction

Fertilization triggers the conversion of two terminally differentiated haploid cells (the sperm and the oocyte) into a diploid totipotent embryo (the zygote). This transition requires a profound reprogramming of many of the cellular pathways operating in the fertilized

oocyte, particularly those impinging on chromatin remodeling, cell cycle control, and gene expression regulation [1]. Collectively, these changes are responsible for the oocyte-to-embryo transition, arguably one of the most dramatic cell fate changes in development.

A central feature of the oocyte-to-embryo transition is the assembly of the zygotic genome. To do so, the fertilized oocyte must merge the sperm-borne paternal genome with its maternal counterpart. Yet, this assembly is hindered by the extremely asymmetric state of parental chromatin at fertilization: The compact paternal chromatin is, in most animal species, histone-depleted and post-meiotic, while maternal chromatin remains histone-associated and meiotically arrested [2,3]. Such asymmetry is resolved by the remodeling of the parental genomes at fertilization [4,5]. In this process, the paternal genome is decondensed through the replacement of the sperm nuclear basic proteins with maternal histones, while the maternal genome completes meiosis. Each of these events leads to the formation of a pronucleus: a nucleosome-based interphasic nucleus containing either the sperm or the oocyte-derived genomic information. The establishment of the functionally equivalent paternal and maternal pronuclei allows the merging, at the first mitotic division, of the parental chromatin into a single zygotic genome.

A remarkable aspect of the oocyte-to-embryo transition is that it occurs in the absence of transcription [6]. Such constrain implies that the molecular determinants driving the acquisition of embryo fate, such as those involved in the assembly of the zygotic genome, must be synthesized during oogenesis and stored in the mature oocyte [7,8]. The genes coding for this unique cell fate transition program are referred to as maternal effect genes: a highly specialized repertoire responsible for priming and sustaining embryo development until the activation of zygotic transcription at the midblastula transition. It can be argued that the expression of these maternal effect genes during oogenesis poses a peculiar challenge to the oocyte. Indeed, developing oocytes must successfully coordinate two gene expression programs with essentially opposing outcomes: one that maintains oocyte fate as the female gamete differentiates, the other responsible for erasing such fate after fertilization.

1 Center for Biomedical Research and Departamento de Ciências Biomédicas e Medicina, Universidade do Algarve, Faro, Portugal

2 Instituto de Medicina Molecular, Faculdade de Medicina, Universidade de Lisboa, Lisboa, Portugal

3 Instituto Gulbenkian de Ciência, Oeiras, Portugal

4 Institute of Biomedicine – iBiMED and Department of Medical Sciences, Universidade de Aveiro, Aveiro, Portugal

*Corresponding author. Tel: +351 934 206 610; E-mail: rgmartinho@ualg.pt

**Corresponding author. Tel: +351 214 464 689; E-mail: navarro-costa@medicina.ulisboa.pt

Recently, the two SET domain-containing methyltransferases, Mixed-lineage leukemia 3 and Mixed-lineage leukemia 4 (collectively referred to as MLL3/4), were shown to control mammalian cell fate transition to the pluripotent state during reprogramming [9]. However, despite being essential for cell fate transition, MLL3/4 were intriguingly dispensable for maintaining cell identity. MLL3/4 are part of the Trithorax group (TrxG) of proteins, a family of chromatin regulators previously proposed to function as maternal effect genes [10]. Based on these observations, we set out to determine the potential role of MLL3/4 in the oocyte-to-embryo transition.

Here, we show that *Drosophila* MLL3/4 (dMLL3/4, also known as Trr) is essential for the transition to embryo fate at fertilization but not for the maintenance of oocyte identity. More specifically, dMLL3/4 is dispensable for normal oocyte differentiation but critically required for the correct assembly of the zygotic genome at fertilization. Such requirement is independent of its methyltransferase activity but relies on the dMLL3/4-mediated regulation of gene expression during oogenesis. Accordingly, we report the identification of a novel oocyte-to-embryo transition gene under direct dMLL3/4 transcriptional control.

Results and Discussion

dMLL3/4 is essential for entry into embryogenesis

dMLL3/4 is an essential gene responsible for the monomethylation of histone H3 lysine 4 (H3K4me1) at enhancers and for the regulated activation of gene expression during development [11–13]. The functions of dMLL3/4 have been evolutionarily conserved [14,15], and this gene has two partially redundant mammalian homologs (MLL3 and MLL4) [16,17], both jointly required for cell fate transition but not for cell identity maintenance [9].

To test the hypothesis that dMLL3/4 promotes the oocyte-to-embryo transition at fertilization, we specifically depleted this chromatin regulator during oogenesis. For this, both an *in vivo* RNA interference (RNAi) approach and germ line mutant clone analysis (induced by the FLP/FRT recombination system) were used. The first approach ensures the post-transcriptional silencing of dMLL3/4 specifically in developing germ cells, while the second induces, in the female germ line, the homozygous mutant state of a previously identified dMLL3/4 null allele (*trr¹*, here referred to as *dml3/4^{-/-}*) [18]. Both approaches resulted in an equally strong depletion of dMLL3/4 in whole ovaries and in early embryos (Fig 1A). This result confirmed that our experimental conditions are associated with a significant reduction of dMLL3/4 levels in the female germ line.

We next tested the effect of dMLL3/4 depletion on female fertility. We observed that, after being mated with wild-type males, < 1% of all eggs laid by dMLL3/4-depleted females could hatch ($n = 543$ and 668 , for the RNAi and *dml3/4^{-/-}* groups, respectively; Fig 1B). This phenotype was limited to the female germ line, as the efficient depletion of dMLL3/4 during sperm differentiation (Fig EV1A) had no obvious effects on male fertility (as assessed by mating dMLL3/4-depleted males with wild-type females; Fig 1B). The origin of the female infertility phenotype could be traced to the fact that dMLL3/4-depleted eggs fail to enter embryogenesis due to an incapability of initiating the embryo mitotic divisions (Fig 1C; $n = 150$ for each tested group).

dMLL3/4 is dispensable for oogenesis

The germ line-specific depletion of dMLL3/4 had no obvious impact on oocyte development. Indeed, ovary morphology and mature egg size were indistinguishable between control and dMLL3/4-depleted conditions (Fig 1D). Supporting this observation, we failed to identify any cytological defects in either the germ cell or somatic compartments of dMLL3/4-depleted ovaries (Figs 1E and EV2). These results are consistent with the previously reported observation that dMLL3/4 only begins to be expressed in late oogenesis (from stage 8 onwards) [18].

The meiotic metaphase I (MI) arrest of mature, non-activated eggs was equally unaffected in the absence of dMLL3/4. More specifically, dMLL3/4 depletion did not disturb the retraction of the meiotic chromosomes into the MI plate ($n = 40$, Fig 1F), nor did it impact prophase I oocyte chromatin architecture ($n = 10$, Fig EV3A).

Collectively, the germ line-specific depletion of dMLL3/4 did not result in any noticeable disturbances in oogenesis, despite critically impairing the entry into embryogenesis. The fact that dMLL3/4 is dispensable for morphologically normal oogenesis contrasts with previous observations for other SET domain histone methyltransferases across different species [19–22].

dMLL3/4 is required for the reprogramming of the paternal genome at fertilization

Why do dMLL3/4-depleted eggs fail to enter embryogenesis? We observed that the depletion of this chromatin remodeler during oogenesis blocks the reprogramming of the paternal genome after fertilization (Fig 2A). More specifically, after being mated with wild-type males, more than 90% of all eggs laid by dMLL3/4-depleted females are unable to convert the tightly compacted sperm-borne paternal genome into the decondensed chromatin of the paternal pronucleus (PN; $n = 36$ and 51 , for the RNAi and *dml3/4^{-/-}* groups, respectively). Indeed, in the absence of dMLL3/4, the sperm genome retains its compact needle-like shape after fertilization, whereas this configuration is rapidly converted into a round decondensed structure in controls (Fig 2A). Given the extremely fast kinetics of *Drosophila* sperm decondensation (in normal conditions, the first zygotic division occurs just 15 min after sperm entry) [23], the previously reported *sra^{-/-}* mutant (*sra^{A108}/sra^{A426}*) was used as control [24]. In this egg activation mutant, the reprogramming of the sperm-borne genome is blocked immediately after decondensation (compare with wild-type male PN in Fig EV3B). Consequently, in fertilized eggs from this genetic background, the paternal genome remains arrested in the shape of the decondensed male PN (Fig 2A).

To understand why the sperm-borne paternal genome fails to be decondensed in dMLL3/4-depleted eggs, RNAi females were mated with males carrying endogenously fluorescent protamine B (ProtB-GFP) [25]. Protamine B is one of the major nuclear proteins incorporated into sperm chromatin during spermatogenesis, and the formation of the decondensed paternal PN after fertilization requires its active removal (alongside other basic nuclear proteins) from the sperm-borne genome [26]. We observed that the depletion of dMLL3/4 during oogenesis resulted in eggs incapable of ensuring protamine removal after fertilization (Fig 2B). Indeed, in more than

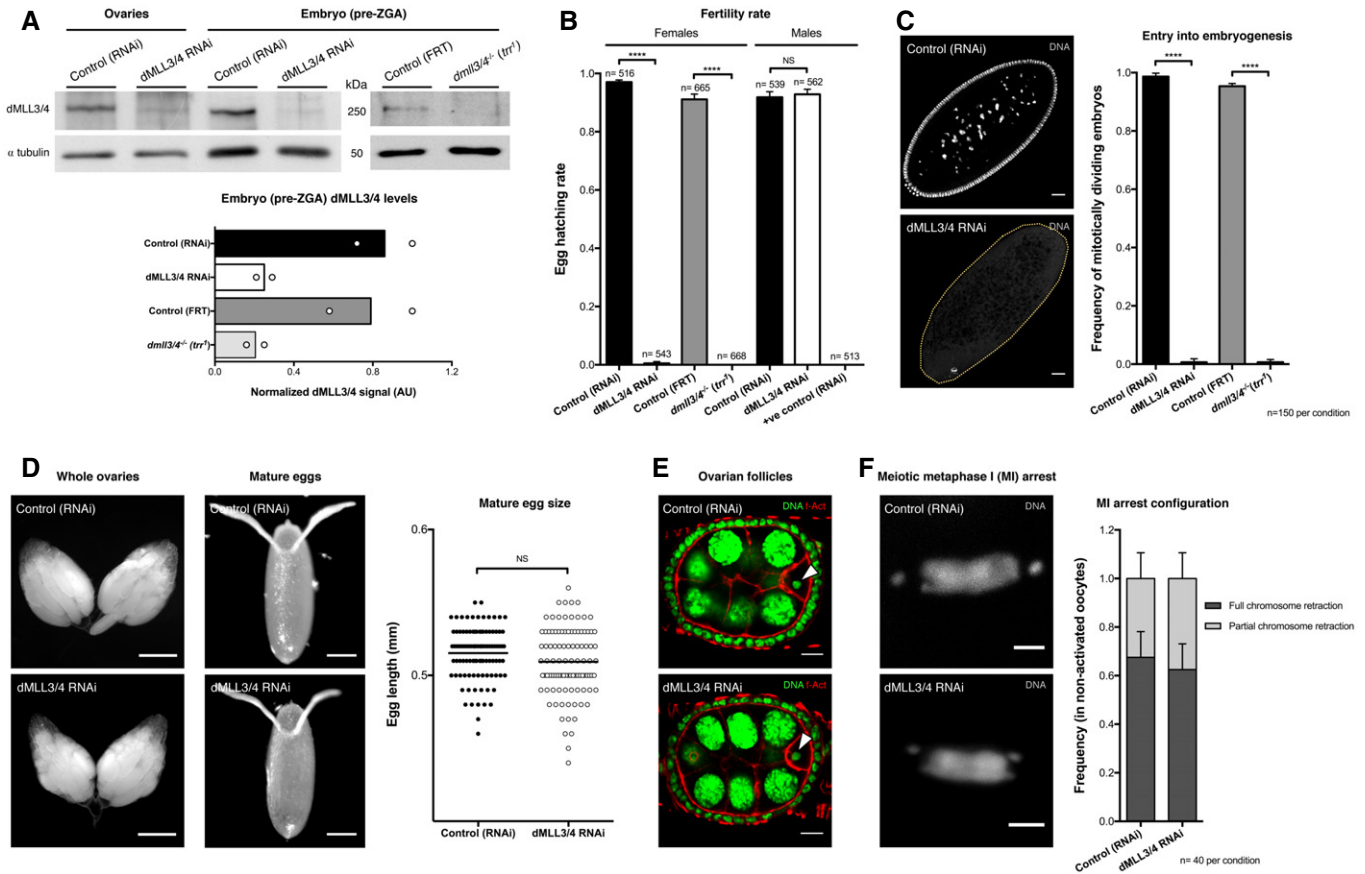


Figure 1. dMLL3/4 is essential for entry into embryogenesis but dispensable for oogenesis.

A dMLL3/4 protein levels are strongly reduced both under germ line-specific RNAi (*nos*-GAL4; UASp-dMLL3/4^{RNAi}) and in a *dml3/4*^{-/-} mutant (*trr*¹). ZGA: zygotic genome activation. The ratio between the dMLL3/4 and α -tubulin signals is expressed in arbitrary units (AU). The results of each independent experiment are plotted, and bars specify mean values.

B dMLL3/4 is essential for female, but not male, fertility. Error bars represent standard deviation, and asterisks indicate significant difference (unpaired *t*-test; *****P* < 0.0001; NS: no significant difference). Results reflect a total of four independent experiments. Male germ line driver: *bam*-GAL4; +ve spermatogenesis control: UASp-Prp19^{RNAi}. See Fig EV1A for the validation of knockdown efficiency in the male germ line.

C dMLL3/4-depleted eggs fail to initiate embryogenesis. The dashed yellow line delimits the egg's cytoplasm. Error bars represent standard deviation, and asterisks indicate significant difference (unpaired *t*-test; *****P* < 0.0001). Results reflect a total of three independent experiments. Scale bar: 30 μ m.

D dMLL3/4 is dispensable for morphologically normal female gonads and gametes. Mature egg size is defined by the length of its main axis and is expressed in millimeters (mm). Quantification of the egg size control group has already been published [30]. Horizontal lines specify mean values. Mann-Whitney *U*-test; NS: no significant difference. Results reflect a total of six independent experiments. Scale bars: 500 and 125 μ m (ovaries and eggs, respectively).

E dMLL3/4 is dispensable for normal ovarian follicle development. Arrowheads point to the oocyte nucleus. F-Act: filamentous actin. Scale bar: 30 μ m. See Fig EV2 for the cytological analysis of additional oogenesis stages.

F dMLL3/4 is dispensable for a normal meiotic metaphase I (MI) arrest. Two different configurations were observed: a tightly packaged chromosome mass (full chromosome retraction) and a more distended plate (partial chromosome retraction, as in the depicted micrographs). Error bars represent standard deviation. Results reflect a total of two independent experiments. Scale bar: 2 μ m. Quantification of the control group has already been published [30]. See Fig EV3A for oocyte chromatin architecture during prophase I.

Source data are available online for this figure.

90% of the fertilized eggs laid by dMLL3/4-depleted females, paternal chromatin retained the ProtB-GFP fluorescent signal (*n* = 44 and 34, for the RNAi and *dml3/4*^{-/-} groups, respectively). In contrast, no ProtB-GFP signal was ever recorded in the control (*sra*^{-/-} mutant; *n* = 43; Fig 2B). Similar to our experiments with wild-type sperm, the genome of ProtB-GFP sperm also remained in a compact configuration in dMLL3/4-depleted eggs, while it was extensively decondensed in controls.

Based on these observations, we conclude that the expression of dMLL3/4 during oogenesis confers oocytes the ability to decondense

the paternal genome after fertilization. The functional basis of this ability resides in the removal of DNA-compacting nuclear proteins from the sperm-borne chromatin.

dMLL3/4 is required for maternal meiotic completion

We found that the role of dMLL3/4 in post-fertilization development went beyond the decondensation of the paternal genome. In fact, dMLL3/4 was also required for the successful completion of female meiosis. Meiotic completion is an essential aspect of the

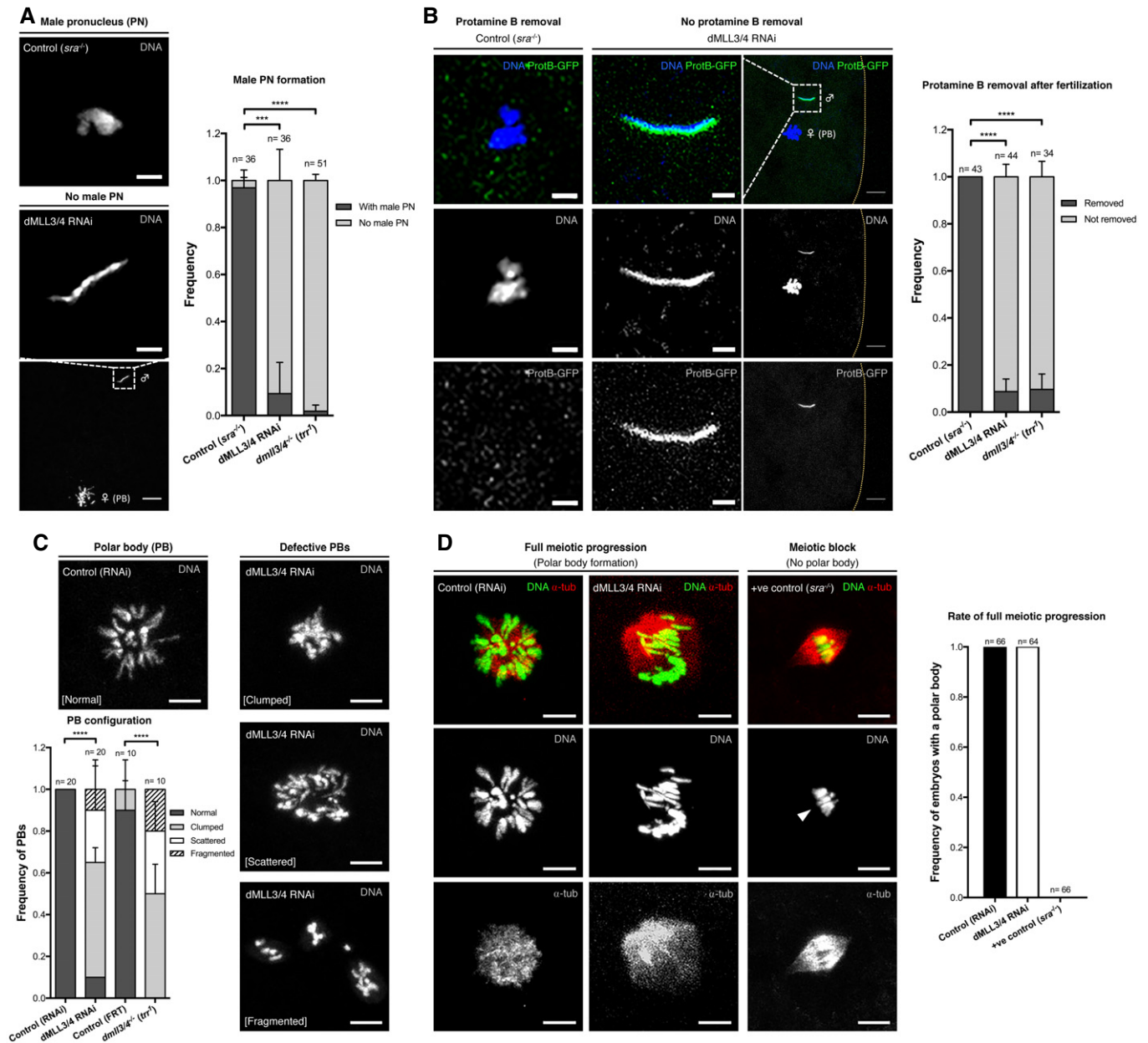


Figure 2. dMLL3/4 is critically required for the remodeling of the two parental genomes at fertilization.

- A dMLL3/4-depleted eggs are incapable of forming the male pronucleus (PN) after fertilization. In such conditions, paternal chromatin (σ) remains in a condensed sperm-like state. The *sra*^{-/-} mutant was used as control for male PN formation. ♀: female meiotic products (polar body: PB). Error bars represent standard deviation, and asterisks indicate significant difference (ANOVA; *****P* < 0.0001; and ****P* = 0.0002). Results reflect a total of four independent experiments. Scale bars: 2 μ m (for σ insets) and 10 μ m.
- B dMLL3/4-depleted eggs are unable to remove protamine B from sperm chromatin. The dashed yellow line delimits the egg's cytoplasm. Error bars represent standard deviation, and asterisks indicate significant difference (ANOVA; *****P* < 0.0001). Results reflect a total of four independent experiments. Scale bars: 2 μ m (for σ insets) and 10 μ m.
- C dMLL3/4 is required for normal female meiotic completion. PB chromatin morphology was used as readout for successful meiotic completion. dMLL3/4 depletion led to significant deviations to the normal PB rosette conformation. Error bars represent standard deviation, and asterisks indicate significant difference (ANOVA; *****P* < 0.0001). Results reflect a total of four independent experiments. Scale bars: 5 μ m.
- D Meiotic progression is not affected in dMLL3/4-depleted eggs. PB formation was used as readout for the progression through the two meiotic divisions. The *sra*^{-/-} mutant was used as positive control for a female meiotic block. Arrowhead: meiosis I-arrested chromatin (compare size with that of PBs). α -tub: α -tubulin. Results reflect a total of four independent experiments. Scale bars: 5 μ m.

oocyte-to-embryo transition: It erases the cell cycle stage asymmetry between the maternal and paternal genomes at fertilization. A particularity of female meiosis is that out of the four resulting

haploid nuclei, only one will contribute to the next generation [27]. All three remaining nuclei (known as polar bodies—PBs) eventually degenerate. In *Drosophila*, these three nuclei fuse, after DNA

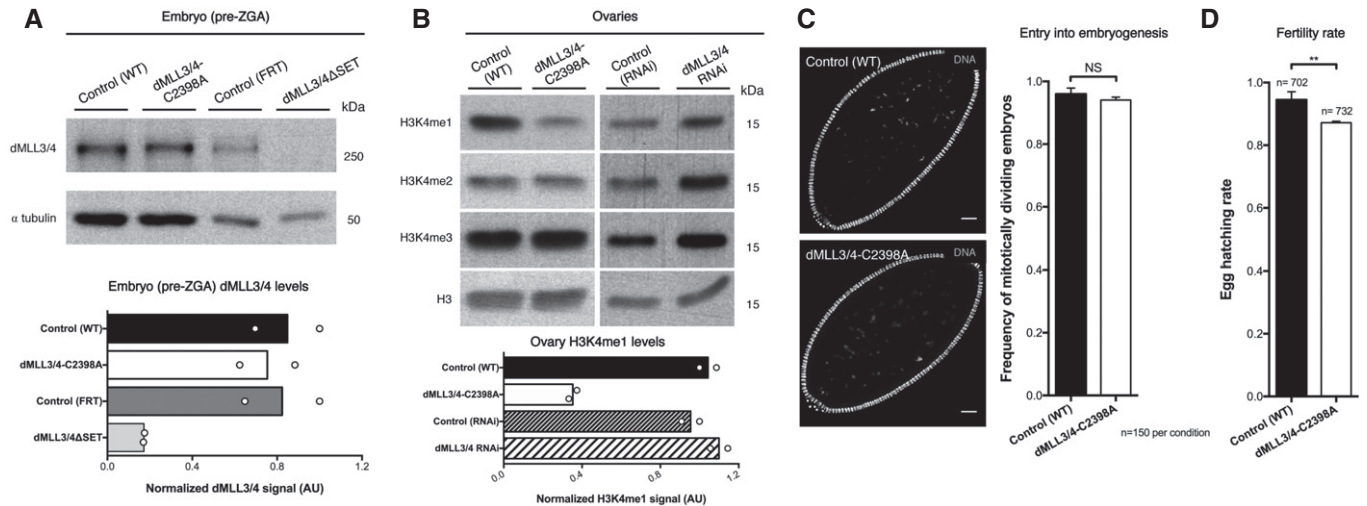


Figure 3. The methyltransferase activity of dMLL3/4 is dispensable for entry into embryogenesis.

- A dMLL3/4 protein levels remain largely unchanged after the substitution of an amino acid in the SET methyltransferase domain (dMLL3/4-C2398A). This allele was inserted into a *dml3/4*^{-/-} background. The insertion of wild-type dMLL3/4 into the same background was used as control [Control (WT)]. Compare with the clear reduction in protein levels observed if the entire SET domain is deleted (dMLL3/4ΔSET, also known as *trr*³). See Fig EV4 for the phenotypical characterization of dMLL3/4ΔSET. ZGA: zygotic genome activation. The ratio between the different dMLL3/4 variants and α -tubulin signals are expressed in arbitrary units (AU). The results of each independent experiment are plotted and bars specify mean values.
- B Ovary H3K4me1 levels are considerably reduced in the catalytically deficient dMLL3/4-C2398A mutant. Such reduction was not observed in the dMLL3/4 RNAi. Protein immunoblots for H3K4me1, me2, and me3 were performed using histone extracts from whole ovaries. The ratio between the H3K4me1 and histone H3 signals was normalized and is expressed in AU. The results of each independent experiment are plotted and bars specify mean values.
- C The initiation of embryogenesis is not affected in the catalytically deficient dMLL3/4-C2398A mutant. Compare with the stark impairment recorded in the dMLL3/4 RNAi (see Fig 1C). Error bars represent standard deviation (unpaired t-test; NS: no significant difference). Results reflect a total of three independent experiments. Scale bar: 30 μ m.
- D dMLL3/4-C2398A is associated with a slight decrease in female fertility. Error bars represent standard deviation, and asterisks indicate significant difference (unpaired t-test; ***P* = 0.0015). Results reflect a total of four independent experiments.

Source data are available online for this figure.

replication, in the cytoplasm of the egg [28,29]. The condensed chromosomes of this single PB organize into a characteristic rosette shape, commonly used as readout for successful meiotic completion (Fig 2C) [30]. dMLL3/4 depletion critically impaired the formation of a normal PB rosette. This PB configuration—indicative of normal meiotic completion—was only detected in < 10% of all dMLL3/4-depleted eggs (*n* = 20 and 10, for the RNAi and *dml3/4*^{-/-} groups, respectively). In all other cases, PB chromatin was severely affected: Chromosomes often collapsed into an indistinct chromatin mass (clumping), failed to properly assemble into a rosette (scattering), or were outright dispersed in the cytoplasm of the egg (fragmentation; Fig 2C). Consistent with these abnormalities, we observed that the four meiotic products were already defective before the formation of the PB rosette, as illustrated by irregularly shaped chromatin and uneven DNA content (Fig EV3C).

Despite these obvious meiotic defects, dMLL3/4-depleted eggs invariably completed meiosis (Fig 2D). In fact, the formation of structurally abnormal PBs in all dMLL3/4-depleted eggs confirmed their capability of progressing, upon egg activation, from the meiotic metaphase arrest to the post-meiotic state (*n* = 64 and 66, for the RNAi and control groups, respectively). This observation stands in stark contrast with egg activation mutants, such as *sra*^{-/-}, which are incapable of progressing from the meiotic metaphase arrest (Fig 2D) [24,31].

Collectively, these observations indicate that the expression of dMLL3/4 during oogenesis does not interfere with meiotic cell cycle progression but is essential for the successful completion of female meiosis.

The methyltransferase activity of dMLL3/4 is dispensable for the oocyte-to-embryo transition

Having established that dMLL3/4 is required for the correct remodeling of both the paternal and maternal genomes at fertilization, we next set out to characterize the mechanistic basis of this requirement. First, we tested whether the H3K4 methyltransferase activity of dMLL3/4 was necessary for the correct acquisition of embryo fate. Since this activity is ensured by a C-terminal SET domain, we initially analyzed a SET domain-deleted dMLL3/4 mutant (dMLL3/4ΔSET, a lethal allele also known as *trr*³) [11,32]. dMLL3/4ΔSET germ line clones largely recapitulated the dMLL3/4 RNAi and null allele phenotypes: Egg hatching was dramatically decreased and fertilized eggs failed to initiate embryogenesis due to defects both in sperm chromatin unpacking and female meiotic completion (Fig EV4). Yet, the deletion of the SET domain had a clear detrimental effect on protein stability, resulting in substantially reduced dMLL3/4 levels in the early embryo (Fig 3A). To avoid this confounding effect, we used the recently published

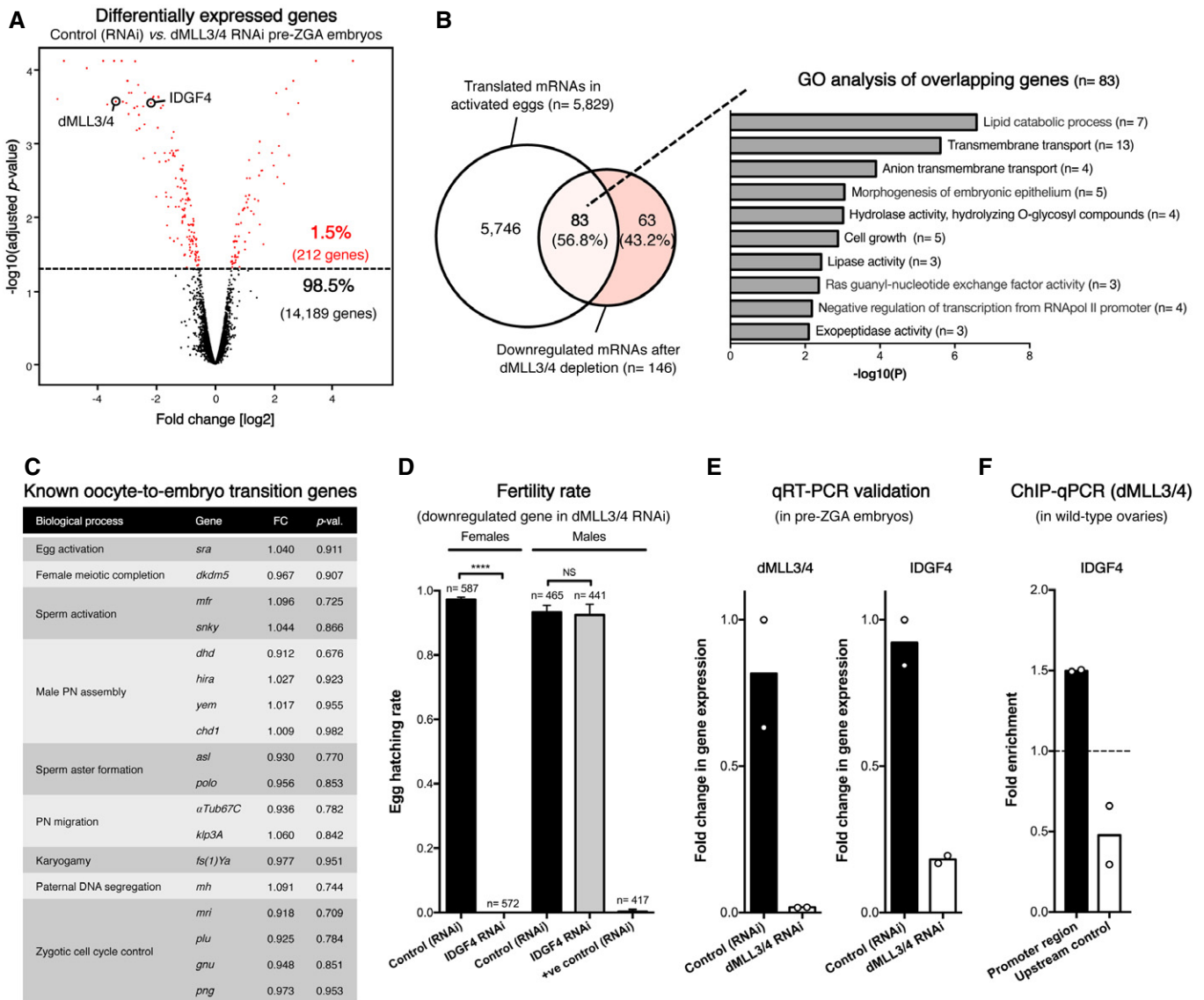


Figure 4. dMLL3/4 defines the expression of a small, functionally coherent maternal gene subset.

- A** Germ line-specific depletion of dMLL3/4 during oogenesis affects a small number of maternal transcripts. Differentially expressed genes are represented in red (adjusted *P*-value cutoff: 0.05). All embryos were manually isolated prior to the onset of zygotic genome activation (pre-ZGA). Results reflect a total of two independent experiments. See panel (E) for qRT-PCR validation of selected genes and the Dataset EV1 for expression values.
- B** The majority of dMLL3/4-activated genes are preferentially translated during egg activation. Gene ontology (GO) analysis of this gene subset identified embryogenesis-related GO terms. Translated mRNAs in activated eggs were extracted from a previously published ribosome footprinting dataset [33].
- C** The expression of known oocyte-to-embryo transition genes is not significantly altered in dMLL3/4-depleted eggs. FC: linear fold change in dMLL3/4 RNAi; *P*-val.: adjusted *P*-value; PN: pronucleus. See the Dataset EV2 for expression values.
- D** IDGF4 is essential for female, but not male, fertility. See Fig 5 for the role of IDGF4 in the oocyte-to-embryo transition. Error bars represent standard deviation, and asterisks indicate significant difference (unpaired *t*-test; *****P* < 0.0001; NS: no significant difference). Results reflect a total of four independent experiments. Male germ line driver: *bam*-GAL4; +ve spermatogenesis control: UASp-Prp19^{RNAi}.
- E** Real-time quantitative reverse transcription PCR (qRT-PCR) validates the downregulation observed in microarray data. Expression levels were normalized against a highly expressed reference gene (Rpl32). The results of each independent experiment are plotted and bars specify mean values.
- F** dMLL3/4 directly binds to the IDGF4 promoter region in ovaries. Chromatin immunoprecipitation coupled to quantitative PCR (ChIP-qPCR) results are presented as fold enrichment relative to a mock ChIP (performed with a pre-immune normal IgG). The upstream control corresponds to an intergenic region ~3 kb away from the IDGF4 promoter. The results of each independent experiment are plotted and bars specify mean values.

dMLL3/4-C2398A mutant [13]. In this mutant, a highly conserved cysteine in the SET domain has been substituted by an alanine, rendering the protein catalytically deficient without affecting its

stability. Indeed, we detected a clear reduction in ovary H3K4me1 despite wild-type-like levels of the dMLL3/4-C2398A protein (Fig 3A and B). Such reduction in methylation did not occur in the

Figure 5. The dMLL3/4-regulated glycosyl hydrolase IDGF4 is a new oocyte-to-embryo transition gene.

- A IDGF4-depleted eggs fail to initiate embryogenesis. Compare with the similar observation recorded in dMLL3/4-depleted eggs (see Fig 1C). Driver: *nos*-GAL4. The dashed yellow line delimits the egg's cytoplasm. Error bars represent standard deviation, and asterisks indicate significant difference (unpaired *t*-test; *****P* < 0.0001). Results reflect a total of three independent experiments. Scale bar: 30 μm.
- B IDGF4 is required for normal maternal meiotic completion. Polar body (PB) chromatin morphology was used as readout for successful meiotic completion. Compare with the similar observation recorded in dMLL3/4-depleted eggs (see Fig 2C). Error bars represent standard deviation, and asterisks indicate significant difference (ANOVA; *****P* < 0.0001). Results reflect a total of four independent experiments. Scale bar: 5 μm.
- C IDGF4-depleted eggs assemble mitotically deficient zygotic chromatin. Such chromatin was arrested at a pre-mitotic state. See Fig EV3D for additional data. Error bars represent standard deviation, and asterisks indicate significant difference (ANOVA; *****P* < 0.0001). Results reflect a total of four independent experiments. Scale bars: 30 μm (egg) and 5 μm (inset).
- D IDGF4 depletion affects the phosphorylation of histone H3 in zygotic chromatin. Although histone H3 serine 10 phosphorylation (pSer10 H3) was virtually undetectable in zygotic chromatin (Z), the same embryos displayed high levels of this modification in their PB chromosomes. Signal quantification is expressed in fluorescence arbitrary units (AU). Horizontal lines specify mean values (*n* = 20). Results reflect a total of two independent experiments. Scale bars: 30 μm (egg) and 5 μm (insets).
- E IDGF4 depletion does not abrogate the acetylation of histone H4 (H4ac) in zygotic chromatin. For comparison, the early zygotic chromatin of control embryos (mitotic cycle 4–6) is depicted. Signal quantification is expressed in fluorescence arbitrary units (AU). Horizontal lines specify mean values (*n* = 20). Results reflect a total of two independent experiments. Scale bars: 5 μm.
- F Proposed model for the dMLL3/4-regulated acquisition of embryo fate at fertilization. As oocytes develop, the Trithorax group protein dMLL3/4 promotes the expression of a small subset of genes. The products of these genes (in red) are dispensable for normal oogenesis, but their storage in the mature oocyte (alongside other maternal effect genes, in gray) is fundamental for the correct assembly of the zygotic genome at fertilization. The glycosyl hydrolase IDGF4 is one of the dMLL3/4-regulated genes critically required for the oocyte-to-embryo transition.

dMLL3/4 RNAi background, suggesting that a redundant mechanism (possibly a distinct methyltransferase) can compensate, in female germ cells, H3K4me1 levels in the absence of dMLL3/4. Nevertheless, we observed that dMLL3/4-C2398A eggs, in contrast to dMLL3/4ΔSET and dMLL3/4 RNAi, had a normal oocyte-to-embryo transition. More specifically, they initiated embryogenesis at a similar rate to that of wild-type controls, despite a slight reduction in hatching rate (Fig 3C and D). The latter was most likely the consequence of the subtle developmental abnormalities previously associated with this background [13].

Taken together, these observations strongly suggest that the methyltransferase activity of dMLL3/4 is dispensable, in unperturbed conditions, for the acquisition of embryo fate.

dMLL3/4 regulates the expression of a functionally coherent gene subset

How does dMLL3/4 regulate the oocyte-to-embryo transition? dMLL3/4 is a transcriptional activator belonging to the TrxG protein family [14,15]. TrxG complexes promote the expression of developmental genes across multiple cellular contexts. Therefore, we hypothesized that dMLL3/4 activates, during oogenesis, the expression of genes that will be later required for post-fertilization development. To test this hypothesis, we performed a transcriptomic analysis of dMLL3/4-depleted eggs. Such analysis revealed that the depletion of dMLL3/4 during oogenesis had a minor effect on the transcriptome: Only 1.5% of the genes were differentially expressed (212 out of 14,401; adjusted *P* < 0.05; Fig 4A). Consistent with the role of dMLL3/4 as a transcriptional activator, the majority (69%) of the differentially expressed genes were downregulated (146 downregulated genes, excluding dMLL3/4, vs. 65 upregulated; Dataset EV1).

Further analysis of the dMLL3/4-defined gene expression program revealed three noteworthy observations. First, the majority (57%) of the dMLL3/4-activated genes are, under normal conditions, translated at the oocyte-to-embryo transition. More specifically, by comparing our transcriptomic data with a previously published ribosome footprinting dataset of activated eggs [33], we

found that 83 out of the 146 downregulated genes were translated at this transition stage (Fig 4B; Dataset EV1). Secondly, consistent with the observed phenotypes, oogenesis-related genes are conspicuously absent from the dMLL3/4-activated gene expression program (Fig 4B). Accordingly, the gene ontology (GO) analysis of the 83 dMLL3/4-activated genes translated at the oocyte-to-embryo transition failed to detect any enrichment for oogenesis-related processes (such as “female gamete generation” or “female meiosis”) [34]. On the other hand, embryogenesis-related GO terms (such as “morphogenesis of embryonic epithelium” and “negative regulation of transcription from RNAPol II promoter”) stood out from the list of enriched terms. Thirdly, dMLL3/4 does not regulate the expression of any gene previously associated with the assembly of the zygotic genome [4,26,30]. In particular, all known *Drosophila* oocyte-to-embryo transition genes were expressed at levels similar to controls (Fig 4C and Dataset EV2).

Based on these data, we conclude that dMLL3/4 promotes, during oogenesis, the expression of a small subset of genes preferentially translated during the acquisition of embryo fate. Could the deregulation of any of them be responsible for the incapability of dMLL3/4-depleted eggs to initiate embryogenesis?

IDGF4 is a new, dMLL3/4-regulated, oocyte-to-embryo transition gene

To address the functional significance of the transcriptomic defects of dMLL3/4-depleted eggs, we individually silenced, during oogenesis, the more severely downregulated genes (Dataset EV3). By analyzing how this silencing affected female fertility, we identified a new oocyte-to-embryo transition gene: imaginal disc growth factor 4 (IDGF4) [35].

The female germ line-specific depletion of IDGF4 (see Fig EV1B for the validation of knockdown efficiency) had a critical impact on fertility: After mating with wild-type males, none of the eggs laid by IDGF4-depleted females hatched (*n* = 572 and 587, for the RNAi and control groups, respectively; Fig 4D). The reduced expression of IDGF4 in dMLL3/4 RNAi eggs was confirmed by real-time quantitative reverse transcription PCR (Fig 4E) and is consistent with the

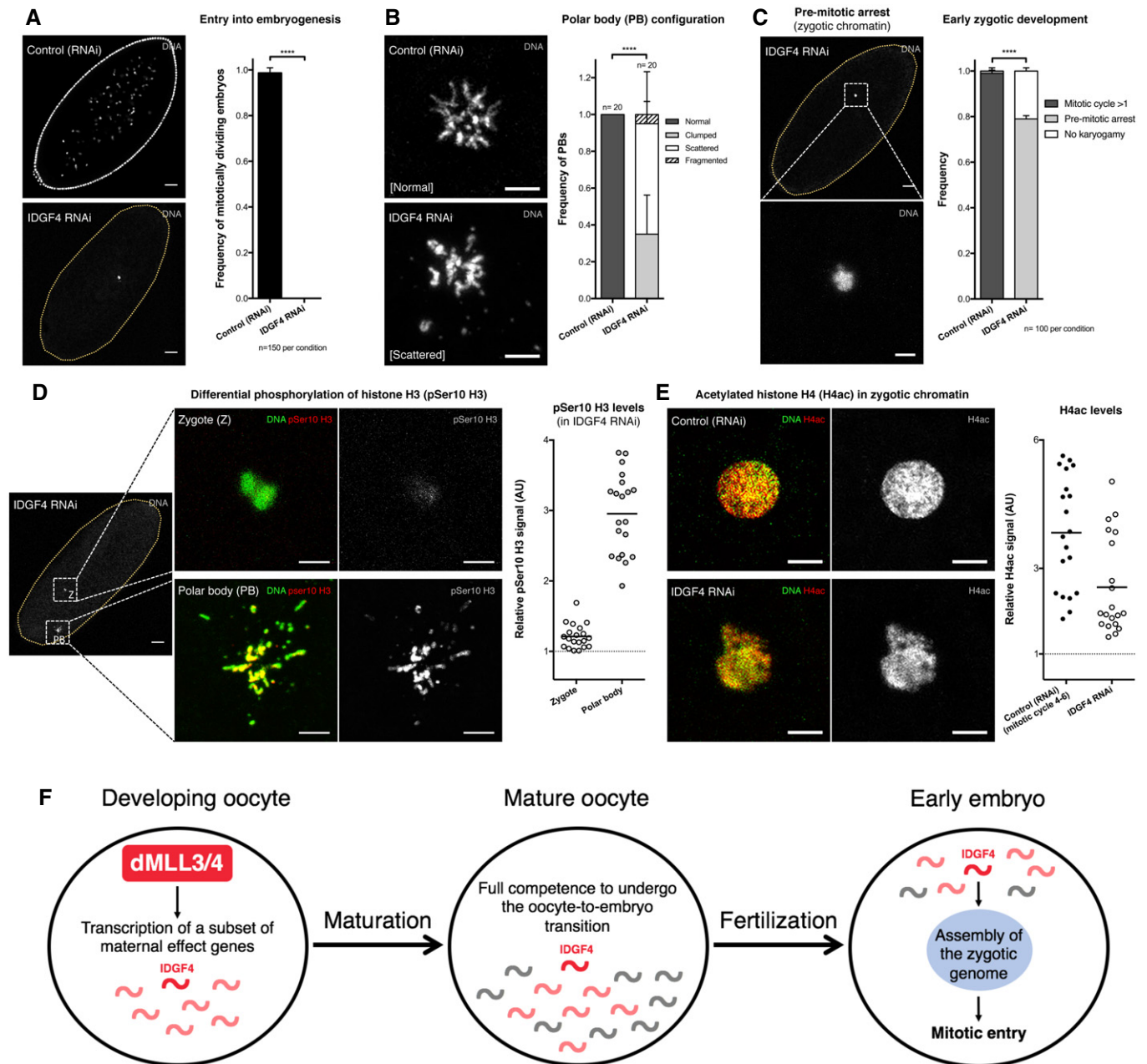


Figure 5.

fact that IDGF4 harbors a predicted Polycomb/Trithorax response element [36]. In accordance, the enrichment of dMLL3/4 in the IDGF4 promoter region (as measured by ovarian tissue chromatin immunoprecipitation coupled to quantitative PCR; Fig 4F) supports the direct binding of dMLL3/4 to IDGF4 in the female germ line, as previously detected in brain tissue [13].

A noteworthy observation was that IDGF4 depletion recapitulated several of the oocyte-to-embryo transition defects of the dMLL3/4 RNAi. More specifically, despite their normal morphology, IDGF4-depleted eggs failed to initiate the embryo mitotic divisions ($n = 150$ for each tested group; Fig 5A, compare with Fig 1C). In addition, these eggs had maternal meiotic completion defects

equivalent to those observed in the dMLL3/4 RNAi. Such defects were illustrated by the clumping, scattering, or outright fragmentation of PB chromosomes ($n = 20$ per group; Fig 5B, compare with Fig 2C).

IDGF4 is one of the six members of the IDGF family of glycosyl hydrolases [35,37]. IDGFs are required for insulin-dependent cell proliferation, polarization, and motility. Their activity has also been linked to developmental processes such as extracellular matrix formation, innate immunity, wound healing, and tissue morphogenesis [38–40]. We observed that IDGF4 is essential for the transition from the meiotic to the mitotic program at fertilization. Indeed, most (78%) IDGF4-depleted eggs assembled zygotic chromatin but were

incapable of initiating mitosis ($n = 100$ for each tested group; Fig 5C). The few eggs that failed to assemble a zygotic genome (“no karyogamy” class in Fig 5C) were characterized by two morphologically equivalent pronuclei that did not appose (Fig EV3D), strongly suggesting that IDGF4 is not required for the decondensation of the paternal genome.

The pre-mitotic arrest of IDGF4-depleted eggs was consistent with barely detectable levels of histone H3 serine 10 phosphorylation (pSer10 H3, a marker of chromosome condensation) in zygotic chromatin ($n = 20$ for each tested group; Fig 5D) [41]. Notably, not only pSer10 H3 was abundantly detected in the polar bodies of the same embryos, but also the levels of acetylated histone H4 (H4ac) were high in the zygotic chromatin of IDGF4-depleted eggs ($n = 20$ for each tested group; Fig 5E). H4ac is one of the first epigenetic marks established in zygotic chromatin, already being detectable at the pronuclear stage [4]. Therefore, the low pSer10 H3 zygotic signal of IDGF4-depleted embryos most likely reflects a mitotic entry defect rather than a generalized deregulation of the post-fertilization epigenome. It should be noted that ectopic expression of IDGF4 during oogenesis (using the GAL4-inducible *Idgf4*^{d00895} allele [42]) was insufficient to visibly rescue the dMLL3/4 RNAi phenotypes (Fig EV5). Under such ectopic expression, the defects in female fertility, initiation of embryogenesis, paternal genome reprogramming, and maternal meiotic completion were largely indistinguishable from those recorded in dMLL3/4-depleted conditions. Based on these observations, we conclude that the nature of the dMLL3/4 phenotype is, most likely, of multigenic origin.

In summary, these data support the notion that IDGF4 is a new, dMLL3/4-regulated, oocyte-to-embryo transition gene. Such observation validates the instructive role of dMLL3/4 in the acquisition of embryo fate.

Conclusions

According to our model, dMLL3/4 regulates, during oocyte development, the expression of a small gene repertoire that is required for the acquisition of embryo fate (Fig 5F). Such regulation may have evolved to better accommodate the expression of specific maternal effect genes within the general transcriptional program of oogenesis. dMLL3/4-mediated gene expression can thus be considered an additional regulatory layer in the complex orchestration of the oocyte-to-embryo transition. Although this transition is largely dependent on the profound post-transcriptional changes taking place at egg activation [33,43,44], our observations emphasize the importance of germ cell transcriptional regulation in the acquisition of embryo fate.

How does dMLL3/4 regulate transcription during oogenesis? Despite containing a H3K4 methyltransferase domain, the catalytic activity of dMLL3/4 is, similarly to other developmental contexts [13], dispensable for both oogenesis and the oocyte-to-embryo transition. dMLL3/4 is part of an evolutionarily conserved multi-protein complex (dMLL3/4-COMPASS) that localizes to enhancer regions of the genome [14,15]. We envisage that enhancers for specific maternal effect genes have a distinct chromatin environment amenable to the binding of dMLL3/4-COMPASS. The possibility that specific gene subsets harbor a defined epigenetic signature in germ cells is not without precedent. Indeed, key

developmental genes have been previously shown to be maintained in a poised epigenetic state in mouse germ cells [45]. Quite fittingly, such epigenetic state is believed to serve as a priming mechanism for the acquisition of totipotency following fertilization [46].

Previous observations suggest that it is the binding at enhancers and not the catalytic activity of dMLL3/4 that is essential for the activation of gene expression. More specifically, in mouse embryonic stem cell (mESC) lines, the recruitment of RNA polymerase II and enhancer RNA synthesis is drastically reduced in the absence of MLL3 and MLL4, but marginally affected in a catalytic dead condition [47]. More recently, it has been proposed, also in mESC lines, that the catalytic activity of MLL3 and MLL4 may in fact facilitate the binding of additional chromatin remodelers to enhancers [48]. Collectively, these observations illustrate the multi-layered role of dMLL3/4-COMPASS in gene expression regulation. A better understanding of such role may be of significance in the context of complex human diseases such as infertility.

Two other TrxG proteins are known to confer oocytes the capability of sustaining post-fertilization development. MLL2 is required during mammalian oogenesis for the subsequent activation of the zygotic genome [20], and we and others have shown that the depletion of dKDM5 in developing *Drosophila* oocytes impairs both the oocyte-to-embryo transition and early embryo development [30,33]. By adding dMLL3/4 to this list, our work underlines the importance of TrxG proteins in the transition to totipotency. In this sense, modulating the expression of TrxG proteins, such as MLL3/4, during somatic cell reprogramming might increase the overall efficiency of this technique. An analogous approach targeting one of the vertebrate orthologs of dKDM5 has already been shown to improve the development of nuclear transfer embryos [49].

The relevance of our findings may even extend to assisted reproduction. We observed that the dMLL3/4-regulated glycosyl hydrolase IDGF4 has a mitogenic effect on the early embryo. The mammalian ortholog of IDGF4 is OVGP1, also known as oviductal glycoprotein 1 [37]. OVGP1 localizes to the oviduct—the site of mammalian fertilization—where it has been shown to be a component of the extracellular matrix of ovulated oocytes and early embryos [50,51]. Despite being important for fertilization and early embryogenesis across different mammalian species, the exact function of OVGP1 remains elusive [52]. Accordingly, OVGP1 has been associated with processes as wide-ranging as sperm capacitation and blastocyst formation [53–55]. Our results indicate that the activation of embryo mitotic divisions is the critical function of IDGF4/OVGP1. Given that IDGF4 has been linked to the acquisition of cellular responsiveness to signaling cues [56], this glycoprotein may be involved in the transduction of fertilization-dependent signals required by the embryo mitotic cascade. In this context, the supplementation of human *in vitro* fertilization (IVF) culture media with OVGP1 may ultimately increase the developmental potential of fertilized oocytes. Indeed, the addition of this extracellular glycoprotein to IVF media has been shown to significantly improve early embryo development rates in several livestock species [57,58]. Bridging such result to the clinical setting could represent an important advance in human assisted reproduction techniques.

Materials and Methods

No statistical methods were used to predetermine sample size. The following assays were intentionally randomized and the investigators blinded to allocation during experiments and outcome assessment: ovary imaging, prophase I oocyte chromatin analysis, characterization of the dMLL3/4 catalytic variants, and the IDGF4 ectopic expression assay.

Drosophila rearing conditions

Drosophila melanogaster flies were raised at 25°C in polypropylene vials (51-mm diameter) containing enriched medium (cornmeal, molasses, yeast, soya flour, and beetroot syrup). For ovary analysis, flies were transferred, 24 h prior to being tested, to polystyrene vials (23.5-mm diameter) containing standard medium (cornmeal, molasses, yeast, and sucrose). For embryo analysis, flies were transferred 48 h before testing to egg laying cages (with 60-mm-diameter apple juice agar plates). In both cases, fresh yeast paste was provided. Tested flies were collected 3–7 days post-eclosion. All females under analysis were kept with wild-type males (Oregon-R) except when they were mated with ProtB-GFP males to assess paternal genome reprogramming at fertilization.

Germ line-specific RNAi

The Gal4-UASp system was used to silence genes of interest specifically in the female germ line [59,60]. In all reported experiments, the silencing was induced from early oogenesis (germ line stem cell) to the mature egg stage, using the well-established *nos*-GAL4 driver [61]. dMLL3/4 was silenced using a publically available UASp-RNAi line (Bloomington stock no. 36916). For the list of UASp-RNAi lines against dMLL3/4-regulated genes, please consult the Dataset EV3. As control, the RNAi response was induced, by *nos*-GAL4, against a sequence not present in the genome of the tested flies (mCherry fluorophore; Bloomington stock no. 35785). For the male fertility tests, selected genes were specifically silenced in the male germ line using *bam*-GAL4, a well-characterized spermatogenesis driver [62].

Maternal mutant generation

The previously published embryonic lethal *trr*¹ null allele was used to generate *dml3/4*^{-/-} maternal mutant embryos [18]. For this, the FLP/FRT *Ovo*^D recombination system was employed [63,64]. Briefly, *Ovo*^D, *FRT101/Y*; *FLP38* males (Bloomington stock no. 1813) were crossed to *trr*¹, *FRT101/FM7* females. Recombination was induced by heat shocking third instar larvae for 1 h at 37°C. For controls, recombination was induced using *FRT101* females (Bloomington stock no. 1844). A similar strategy was employed for the SET domain-deleted *trr*³ allele (dMLL3/4ΔSET) [11].

Additional Drosophila strains

Two previously published loss-of-function alleles affecting the *Drosophila* calcipressin gene *sarah* (*sra*^{A108} and *sra*^{A426}) were used to generate the *sra*^{-/-} egg activation mutant (*sra*^{A108/sra}^{A426} transheterozygote) [24]. The reprogramming of the paternal genome

after fertilization was tested by mating females under analysis with ProtB-GFP males carrying a fusion of Protamine B with enhanced green fluorescent protein (*Sp/CyO*; *ProtB-GFP*) [25]. An UASp fly stock carrying a double-stranded RNA against an essential gene (the spliceosome subunit *Prp19*) was used as positive control for spermatogenesis phenotypes [65]. To test the functional significance of the dMLL3/4 methyltransferase activity without affecting protein stability, we used the previously published dMLL3/4-C2398A catalytically deficient allele (inserted into the *dml3/4*^{-/-} background) [13]. A wild-type dMLL3/4 transgene in the same background served as control. For the IDGF4 addback experiment, one copy of a GAL4-inducible allele carrying a P{XP} transgene in its 5' UTR (*Idgf4*^{d00895}) was inserted into the dMLL3/4 RNAi background [42].

Antibodies

The following primary antibodies were used for immunofluorescence: mouse anti- α -tubulin (1:500 dilution, Sigma T9026); mouse anti-Orb (clones 4H8 and 6H4, 1:30 dilution each, Developmental Studies Hybridoma Bank); rabbit anti-pSer10 H3 (1:500 dilution, Upstate 06-570); and rabbit anti-H4ac (1:500 dilution, Millipore 06-866). The following primary antibodies were used for immunoblotting: rabbit anti-dMLL3/4 (1:1,000 dilution, from both the Alexander Mazo and Ali Shilatifard laboratories) [11,12]; rabbit anti-H3K4me1 (1:5,000 dilution, Active Motif 39298); rabbit anti-H3K4me2 (1:2,000 dilution, Active Motif 39142); rabbit anti-H3K4me3 (1:5,000 dilution, Active Motif 39160); rabbit anti-H3 (1:8,000 dilution, Cell Signalling Technology #9715); and mouse anti- α -tubulin (1:50,000 dilution, Sigma T6199).

Secondary detection was performed with Cy3, Cy5, and HRP-conjugated antibodies at 1:1,000 (immunofluorescence) and 1:4,000 (immunoblotting) dilutions (Jackson ImmunoResearch).

Protein immunoblotting

Maternal protein extracts were prepared from pre-zygotic genome activation (ZGA) embryos as previously described [30,65]. Briefly, early embryos (< 1 h post-laying) were dechorionated with a 50% commercial bleach solution and manually selected for the lack of morphological hallmarks of a post-ZGA state (selection for the absence of pole cells and cortical nuclei). Maternal protein extracts were obtained by lysing the embryos with a needle in Laemmli sample buffer and heating for 5 min at 100°C. Fifteen embryos were selected per genotype per experiment. Ovary protein extracts were enriched for core histones using a histone purification mini kit (Active Motif). Twenty ovary pairs were included per sample.

Protein samples were run on 6% or 15% SDS-PAGE gels (for dMLL3/4 and H3K4 methylation analysis, respectively) and transferred to nitrocellulose membranes (Amersham) for 1 h at 100 V. Membranes were blocked for 1 h at room temperature in 5% non-fat milk in PBS-T [0.1% Tween-20 in PBS (both from Sigma-Aldrich)], followed by an overnight incubation with the primary antibody (at 4°C) in 1% non-fat milk in PBS-T. After washing, membranes were blocked for 15 min in 5% non-fat milk in PBS-T and then incubated for 2 h (at room temperature) with the secondary antibody in 1% non-fat milk in PBS-T. Following another round of washing, membranes were incubated with ECL solution

for 1 min. Protein detection was performed using a ECL Hyperfilm (Amersham).

Fertility tests

Fertility was tested as previously described [30]. In either male or female fertility tests, egg laying cages with 20 females and 10 males were maintained at 25°C for 48 h prior to analysis. Tested genotypes were mated with a wild-type strain (Oregon-R). All flies were 3–7 days post-eclosion, and analyses were performed on two consecutive days. Laid eggs were collected for 30 min in apple juice agar plates and further incubated for 48 h at 25°C. The total number of eggs and the number of hatched eggs were recorded upon collection and 48 h afterward, respectively. Fertility rate was determined as the number of hatched eggs divided by the total number of eggs.

Embryo imaging

Egg laying cages with 40 females and approximately 20 males were maintained at 25°C for 48 h prior to analysis. Embryos were collected in apple juice agar plates (up to 30 min after egg laying) and immediately processed. Collection times went up to 1 h after egg laying followed by 2 additional hours of incubation at 25°C when assessing entry into embryogenesis. Embryo processing started with dechorionation in a 50% commercial bleach solution. Embryos were then fixed and devitellinized in a 1:1 heptane-methanol mix for 5 min with shaking. Following rehydration, embryos were stained as previously described [66]. Briefly, embryos were blocked for 1 h in BBT [PBS-T supplemented with 1% (w/v) bovine serum albumin and 1% (w/v) donkey serum (both from Sigma-Aldrich)]. Primary antibody incubation was performed overnight at 4°C in BBT. After washing, embryos were incubated in the secondary antibody solution (in BBT, for 1 h at room temperature). DNA was stained either with SYTOX Green (Invitrogen) or Hoechst 33342 (Thermo Fisher). For SYTOX Green, embryos were incubated for 30 min in a 1:5,000 dilution in PBS-T supplemented with 5 µg/ml RNase A (Sigma-Aldrich). For Hoechst 33342, the incubation time for a 5 µg/ml solution in PBS-T was 10 min. Embryos were mounted in fluorescence mounting medium (Dako), and images were acquired with either a 40× HCX PL APO CS oil immersion objective (numerical aperture: 1.25–0.75) or a 63× HCX PL APO oil immersion objective (numerical aperture: 1.40–0.60) on a Leica SP5 confocal microscope.

For the measurement of mature eggs, these were photographed (after a 1 h collection) using a camera-coupled Leica MZ12.5 stereomicroscope (Plan APO 1.0× objective, amplification: 64×). Egg size corresponds to the length of its main axis, as measured using the ImageJ software (v1.48i; National Institutes of Health). Since this experiment (Fig 1D) was part of a larger dataset, the quantification of the control group has already been published [30].

Ovary imaging

Adult ovaries (10 ovary pairs per sample per experiment) were processed as previously described [30]. Briefly, ovaries were dissected in PBS and fixed for 20 min in a heptane-fixative mix at 3:1. The fixative consisted of 4% formaldehyde (Polysciences) in a PBS + 0.5% NP-40 (Sigma-Aldrich) solution. The ovarioles were

partly detached, and ovaries were incubated for 2 h in PBS-T (0.2% Tween-20) supplemented with 1% Triton X-100 (Sigma-Aldrich), 1% (w/v) bovine serum albumin and 1% (w/v) donkey serum. Primary antibody incubation was performed overnight at 4°C in BBT. The following day, ovaries were washed and incubated for 1 h at room temperature in the secondary antibody solution (in BBT). Filamentous actin (f-Act) was stained with phalloidin-TRITC (Sigma-Aldrich) at 1:200 in PBS-T for 20 min. DNA was stained with SYTOX Green, and the ovaries were mounted in fluorescence mounting medium. Fluorescence images were acquired with the previously described set-up (see “Embryo immunofluorescence”). For the bright-field imaging of whole ovaries, these were photographed after fixation using a camera-coupled Leica MZ12.5 stereomicroscope.

Meiotic metaphase I arrest analysis

A protocol preventing egg activation was used to analyze the true metaphase I arrest configuration of the mature *Drosophila* female gamete [30,67]. Briefly, virgin females were aged, in the absence of males, for 4 days in standard medium supplemented with fresh yeast paste. Ovaries (10 pairs per sample per experiment) were quickly dissected in modified Robb's medium and immediately transferred to fixative (4% formaldehyde in Robb's medium). After a 5-min incubation, ovaries were washed and DNA was stained with SYTOX Green. Since this experiment (Fig 1F) was part of a larger dataset, the quantification of the control group has already been published [30].

Prophase I oocyte chromatin architecture analysis

The entire chromatin volume of individual prophase I oocytes was acquired as 0.5-µm-thick slices using a Leica SP5 confocal microscope (in fluorescence mounting medium). Two developmental stages were selected: before and after the establishment of the prophase I arrest (stages 1 and 6, respectively). Orb staining was used to unequivocally distinguish stage 1 oocytes from other neighboring cells. Slices were stacked into maximum intensity Z-projections and binarized using an automated global thresholding method (Li's minimum cross entropy thresholding; ImageJ). The perimeter of the binarized chromatin signal was then measured.

Gene expression analysis

After manual isolation of pre-ZGA embryos (see “Protein immunoblotting”), total RNA was extracted using the PureLink RNA Mini Kit (Ambion). Total RNA was then processed for hybridization onto *Drosophila* Gene 1.1 ST Array Strip (Affymetrix) according to manufacturer's instructions. For this, a GeneChip WT PLUS Reagent Kit (Affymetrix) and a GeneAtlas Hybridization, Wash and Stain Kit for WT Array Strips (Affymetrix) were used. One hundred nanograms of total RNA containing spiked in Poly-A RNA controls (GeneChip Poly-A RNA Control Kit, Affymetrix) were reverse transcribed for synthesis of single-stranded cDNA. After second-strand synthesis, the obtained double-stranded cDNA served as template for an *in vitro* transcription reaction to generate amplified cRNA. Fifteen micrograms of purified cRNA was then used for a second cycle of single-strand cDNA synthesis, after which 5.5 µg of ss-cDNA was

fragmented and end-labeled. During this process, checkpoints for purity as well as integrity and size distribution of cRNA and fragmented ss-cDNA were performed using NanoDrop 1000 Spectrophotometer and Bioanalyzer 2100, respectively. Finally, 3.5 µg of the amplified, fragmented, and labeled ss-cDNA was prepared in a 150 µl hybridization cocktail (containing hybridization controls) and 120 µl was used for the hybridization. The array strips were subsequently washed, double-stained, and scanned. The hybridization, washing, and scanning were performed using the Affymetrix GeneAtlas System. For total RNA extraction from testes (PureLink RNA Mini Kit), 30 gonads were dissected from 3 to 7 days post-eclosion males.

The expression level of selected transcripts was validated by real-time quantitative reverse transcription PCR (qRT-PCR) in both testes and pre-ZGA embryos. One µg of total RNA was used for reverse transcription with Oligo(dT)₁₈ primers (Transcriptor First Strand cDNA Synthesis Kit, Roche). qRT-PCR was performed under standard conditions using the Power SYBR Green PCR Master Mix (Applied Biosystems) in an ABI QuantStudio 7 station (Applied Biosystems). Samples were normalized using the expression of the Ribosomal protein L32 (*RpL32*) housekeeping gene. Relative expression levels were calculated with the $2^{-\Delta\Delta CT}$ method, as previously described [68]. Primers were designed with Primer-BLAST (<https://www.ncbi.nlm.nih.gov/tools/primer-blast/>), and the corresponding sequences are as follows: dMLL3/4_F: ATGCAGCTCGGGACA TTGAA; dMLL3/4_R: ATGCCACGGTCTTGGACTC; IDGF4_F: ACT CTTCGCTGTTCTTCGATGT; IDGF4_R: CGTCTCGTTCAGTCTCGTAG AT; RpL32_F: GCAAGCCCAAGGGTATCGA; and RpL32_R: CGATGT TGGCATCAGATACTG.

Ovary chromatin immunoprecipitation

Chromatin immunoprecipitation (ChIP) was performed based on a fast ChIP method [69]. For each reaction, approximately 200 manually dissected ovaries from 3 to 7 days post-eclosion females (tissue volume: ~100 µl) were included. Briefly, ovaries were cross-linked with 1.8% formaldehyde in A1 buffer [60 mM KCl, 15 mM NaCl, 15 mM HEPES (pH 7.6), 4 mM MgCl₂, 0.5% Triton X-100, 0.5 mM DTT, supplemented with an EDTA-free protease inhibitor cocktail (Sigma-Aldrich)] and homogenized with a Dounce homogenizer (type A pestle, for a total of 10 strokes). After a 15-min incubation at room temperature, the cross-linking was stopped by adding glycine (final concentration: 225 mM, 5-min quenching). Nuclei were pelleted by centrifugation (4,000 g for 5 min at 4°C), and the resulting pellet was washed three times in A1 buffer and once in A2 buffer [140 mM NaCl, 15 mM HEPES (pH 7.6), 1 mM EDTA, 0.5 mM EGTA, 1% Triton X-100, 0.5 mM DTT, 0.1% sodium deoxycholate, supplemented with protease inhibitor (Sigma-Aldrich)]. The nuclei were then resuspended in A2 buffer with 0.1% SDS and 0.5% N-lauroylsarcosine. Sonication was performed, on ice, with a Soniprep 150 (MSE) under the following conditions: Five pulses of 10 s (amplitude: 7 µm) interspersed by 30-s intervals. The fragmented chromatin (DNA fragment size range: 200–400 bp) was then recovered by high-speed centrifugation.

For the input control, 40 µl (1:10) of chromatin was incubated overnight (at 65°C) in A3 buffer (A2 buffer supplemented with 0.05% SDS and NaCl to a final concentration of 320 mM). The next day, proteinase K (Thermo Scientific) was added and the solution

was incubated for further 2 h at 45°C. A phenol–chloroform DNA extraction was then performed.

For each immunoprecipitation, 500 µl of chromatin was diluted in A2 buffer (final volume: 1 ml) and pre-incubated for 1 h at 4°C with 20 µl Dynabeads Protein G (Invitrogen). Antibodies (either a dMLL3/4 antibody or a pre-immune normal IgG mock ChIP control) were added following bead removal. Samples were then incubated overnight at 4°C, and, on the next day, Dynabeads Protein G was added for an additional 2-h incubation. After washing (four times in A3 buffer and twice in TE buffer), chromatin was incubated with proteinase K for 1 h at 55°C. Elution was then performed by adding 10% Chelex-100 (Bio-Rad) to the beads.

For quantitative PCR, primers were designed based on a dMLL3/4 ChIP-seq dataset in adult *Drosophila* brain tissue [13]. This dataset guided the selection of two regions to be amplified: one in the previously detected dMLL3/4 peak at the IDGF4 promoter, the other in an upstream intergenic control region (~3 kb away from the peak and with no recorded dMLL3/4 signal). Primer sequences are as follows: IDGF4_peak_F: GAATACGAAACCGGCAAGAC; IDGF4_peak_R: TTTATTCTCGCTGCGTTCGCT; IDGF4_upstream_control_F: GCAGTTGTGGACGATTCGATG; and IDGF4_upstream_control_R: CGTGAGAGTGAGAAAGGTGTGA. qRT-PCR was performed as before, using the Power SYBR Green PCR Master Mix in an ABI QuantStudio 7 station. Results are expressed as fold enrichment relative to a mock ChIP (performed with a pre-immune normal IgG).

Embryo chromatin signal quantification

The entire volume of zygotic (cycle 1 or cycles 4–6) and polar body chromatin was acquired as 1-µm-thick slices using a Leica SP5 confocal microscope. Slices corresponding to each nucleus were stacked into a single maximum intensity Z-projection using ImageJ, and the limits of the chromatin area were defined. The mean fluorescence value of the tested signals was then recorded in arbitrary units (AU) inside the defined area, alongside that of a background reading. Relative signals were calculated as the mean fluorescence of the chromatin signal divided by the mean fluorescence of the corresponding background.

Statistical analysis

The scanned arrays were analyzed with Affymetrix Expression Console software using Robust Multi-array Analysis for both quality control and to obtain expression values. Control probe sets were removed, and log₂ expression values of the remaining 15,308 transcripts were imported into Chipster 3.8.1 [70]. Differential expression was determined by empirical Bayes two-group test with Benjamini-Hochberg multiple testing correction and a *P*-value cut-off of 0.05 [71].

Gene ontology analysis was performed using the Metascape Gene Annotation and Analysis Resource tool (<http://metascape.org/gp/index.html#/main/step1>) using the “express analysis” settings [72].

Nonparametric tests (Mann–Whitney *U*-test) were used to compare egg size, relative fluorescence signals, and chromatin perimeter measurements between groups. For egg eclosion and mitotic entry rates, unpaired (two sample) *t*-tests were used. The comparison of male PN configuration, sperm ProtB-GFP signal,

meiotic completion, MI arrest configuration, and early zygotic development between groups was performed by two-way ANOVA. Reported *P*-values correspond to two-tailed tests. All analyses were performed using Prism 7 software (GraphPad).

Data availability

All relevant data and reagents are available from the authors. The microarray data discussed in this publication have been deposited in NCBI's Gene Expression Omnibus [73] and are accessible through GEO Series accession number GSE108033 (<https://www.ncbi.nlm.nih.gov/geo/query/acc.cgi?acc=GSE108033>).

Expanded View for this article is available online.

Acknowledgements

The authors wish to thank Gabriel Martins and Nuno Pimpão for assistance in fluorescence microscopy. We acknowledge Ali Shilatifard (Northwestern University Feinberg School of Medicine, Chicago, USA) for kindly providing us the dMLL3/4 catalytically deficient fly stock (and its control), as well as for an aliquot of the anti-dMLL3/4 antibody. We also thank Alexander Mazo (Thomas Jefferson University, Philadelphia, USA) for both the *trr¹* and *trr³* fly stocks and anti-dMLL3/4 antibody. Renate Renkawitz-Pohl (Philipps-Universität Marburg, Germany) and Mariana Wolfner (Cornell University, Ithaca, USA) kindly provided us with the ProtB-GFP and *sarah* mutant fly stocks, respectively. We acknowledge the TRiP at Harvard Medical School (NIH/NIGMS R01-GM084947) for providing several of the transgenic RNAi fly stocks used in this study. We thank the labs of Raquel Oliveira (Instituto Gulbenkian de Ciência) and Maria Carmo-Fonseca (Instituto de Medicina Molecular) for their technical assistance. The Microscopy Unit was partially supported by Portuguese National Funding (FCT: PPBI-POCI-01-0145-FEDER-022122). This work was developed with the support of the Research Infrastructure Congento (project LISBOA-01-0145-FEDER-022170). Rui G. Martinho is supported by Portuguese national funding through the following FCT grants: PTDC/BEX-BID/0395/2014 and UID/BIM/04773/2013 CBMR 1334. Jörg D. Becker received salary support from FCT through an "Investigador FCT" position (IF/01341/2012). Paulo Navarro-Costa is supported by a FCT Postdoctoral fellowship (SFRH/BPD/84214/2012).

Author contributions

PP: Investigation. LGG: Investigation. JS: Investigation. JDB: Investigation, Writing (review & editing). RGM: Conceptualization, Writing (review & editing), Funding acquisition. PN-C: Conceptualization, Investigation, Writing (original draft + review & editing).

Conflict of interest

The authors declare that they have no conflict of interest.

References

- Clift D, Schuh M (2013) Restarting life: fertilization and the transition from meiosis to mitosis. *Nat Rev Mol Cell Biol* 14: 549–562
- Morgan HD, Santos F, Green K, Dean W, Reik W (2005) Epigenetic reprogramming in mammals. *Hum Mol Genet* 14 (Spec No. 1): R47–R58
- Burton A, Torres-Padilla M-E (2014) Chromatin dynamics in the regulation of cell fate allocation during early embryogenesis. *Nat Rev Mol Cell Biol* 15: 723–734
- Loppin B, Dubruielle R, Horard B (2015) The intimate genetics of *Drosophila* fertilization. *Open Biol* 5: 150076
- Albert M, Peters AHFM (2009) Genetic and epigenetic control of early mouse development. *Curr Opin Genet Dev* 19: 113–121
- Lipshitz HD (2015) *The maternal-to-zygotic transition*. Amsterdam, The Netherlands: Academic Press
- Johnston DS, Nüsslein-Volhard C (1992) The origin of pattern and polarity in the *Drosophila* embryo. *Cell* 68: 201–219
- Li L, Zheng P, Dean J (2010) Maternal control of early mouse development. *Development* 137: 859–870
- Wang C, Lee J-E, Lai B, Macfarlan TS, Xu S, Zhuang L, Liu C, Peng W, Ge K (2016) Enhancer priming by H3K4 methyltransferase MLL4 controls cell fate transition. *Proc Natl Acad Sci USA* 113: 11871–11876
- Andreu-Vieyra C, Matzuk MM (2007) Epigenetic modifications by Trithorax group proteins during early embryogenesis: do members of Trx-G function as maternal effect genes? *Reprod Biomed Online* 14: 201–207
- Sedkov Y, Cho E, Petruk S, Cherbas L, Smith ST, Jones RS, Cherbas P, Canaani E, Jaynes JB, Mazo A (2003) Methylation at lysine 4 of histone H3 in ecdysone-dependent development of *Drosophila*. *Nature* 426: 78–83
- Herz HM, Mohan M, Garruss AS, Liang K, Takahashi YH, Mickey K, Voets O, Verrijzer CP, Shilatifard A (2012) Enhancer-associated H3K4 monomethylation by Trithorax-related, the *Drosophila* homolog of mammalian Mll3/Mll4. *Genes Dev* 26: 2604–2620
- Rickels R, Herz H-M, Sze CC, Cao K, Morgan MA, Collings CK, Gause M, Takahashi Y-H, Wang L, Rendleman EJ et al (2017) Histone H3K4 monomethylation catalyzed by Trr and mammalian COMPASS-like proteins at enhancers is dispensable for development and viability. *Nat Genet* 49: 1647–1653
- Schuettengruber B, Bourbon H-M, Di Croce L, Cavalli G (2017) Genome regulation by polycomb and trithorax: 70 years and counting. *Cell* 171: 34–57
- Piunti A, Shilatifard A (2016) Epigenetic balance of gene expression by Polycomb and COMPASS families. *Science* 352: aad9780
- Tan YC, Chow VT (2001) Novel human HALR (MLL3) gene encodes a protein homologous to ALR and to ALL-1 involved in leukemia, and maps to chromosome 7q36 associated with leukemia and developmental defects. *Cancer Detect Prev* 25: 454–469
- FitzGerald KT, Diaz MO (1999) MLL2: a new mammalian member of the trx/MLL family of genes. *Genomics* 59: 187–192
- Sedkov Y, Benes JJ, Berger JR, Riker KM, Tillib S, Jones RS, Mazo A (1999) Molecular genetic analysis of the *Drosophila* trithorax-related gene which encodes a novel SET domain protein. *Mech Dev* 82: 171–179
- Brici D, Zhang Q, Reinhardt S, Dahl A, Hartmann H, Schmidt K, Goveas N, Huang J, Gahurova L, Kelsey G et al (2017) The histone 3 lysine 4 methyltransferase Setd1bis is a maternal effect gene required for the oogenic gene expression program. *Development* 144: 2606–2617
- Andreu-Vieyra CV, Chen R, Agno JE, Glaser S, Anastasiadis K, Stewart AF, Matzuk MM (2010) MLL2 is required in oocytes for bulk histone 3 lysine 4 trimethylation and transcriptional silencing. *PLoS Biol* 8: e1000453-19
- Yan D, Neumüller RA, Buckner M, Ayers K, Li H, Hu Y, Yang-Zhou D, Pan L, Wang X, Kelley C et al (2014) A regulatory network of *Drosophila* germline stem cell self-renewal. *Dev Cell* 28: 459–473
- Xiao Y, Bedet C, Robert VJP, Simonet T, Dunkelbarger S, Rakotomalala C, Soete G, Korswagen HC, Strome S, Palladino F (2011) *Caenorhabditis elegans* chromatin-associated proteins SET-2 and ASH-2 are differentially required for histone H3 Lys 4 methylation in embryos and adult germ cells. *Proc Natl Acad Sci USA* 108: 8305–8310

23. Foe VF, Odell GM, Edgar BA (1993) Mitosis and morphogenesis in the *Drosophila* embryo: point and counterpoint. In *The Development of Drosophila melanogaster*, Bate M, Arias AM (eds), pp 149–300. Cold Spring Harbor, NY: Cold Spring Harbor Laboratory Press
24. Horner VL, Czank A, Jang JK, Singh N, Williams BC, Puro J, Kubli E, Hanes SD, McKim KS, Wolfner MF et al (2006) The *Drosophila* calcipressin sarah is required for several aspects of egg activation. *Curr Biol* 16: 1441–1446
25. Jayaramaiah Raja S, Renkawitz-Pohl R (2005) Replacement by *Drosophila melanogaster* protamines and Mst77F of histones during chromatin condensation in late spermatids and role of sesame in the removal of these proteins from the male pronucleus. *Mol Cell Biol* 25: 6165–6177
26. Tirmarche S, Kimura S, Dubrulle R, Horard B, Loppin B (2016) Unlocking sperm chromatin at fertilization requires a dedicated egg thioredoxin in *Drosophila*. *Nat Commun* 7: 13539
27. Li R, Albertini DF (2013) The road to maturation: somatic cell interaction and self-organization of the mammalian oocyte. *Nat Rev Mol Cell Biol* 14: 141–152
28. Huettnner AF (1924) Maturation and fertilization in *Drosophila melanogaster*. *J Morphol* 39: 249–265
29. Page AW, Orr-Weaver TL (1997) Activation of the meiotic divisions in *Drosophila* oocytes. *Dev Biol* 183: 195–207
30. Navarro-Costa P, McCarthy A, Prudêncio P, Greer C, Guilgur LG, Becker JD, Secombe J, Rangan P, Martinho RG (2016) Early programming of the oocyte epigenome temporally controls late prophase I transcription and chromatin remodelling. *Nat Commun* 7: 12331
31. Takeo S, Tsuda M, Akahori S, Matsuo T, Aigaki T (2006) The calcineurin regulator sra plays an essential role in female meiosis in *Drosophila*. *Curr Biol* 16: 1435–1440
32. Tie F, Banerjee R, Saiakhova AR, Howard B, Monteith KE, Scacheri PC, Cosgrove MS, Harte PJ (2014) Trithorax monomethylates histone H3K4 and interacts directly with CBP to promote H3K27 acetylation and antagonize Polycomb silencing. *Development* 141: 1129–1139
33. Kronja I, Yuan B, Eichhorn SW, Dzeky K, Krijgsveld J, Bartel DP, Orr-Weaver TL (2014) Widespread changes in the posttranscriptional landscape at the *Drosophila* oocyte-to-embryo transition. *Cell Rep* 7: 1495–1508
34. Baker DA, Russell S (2009) Gene expression during *Drosophila melanogaster* egg development before and after reproductive diapause. *BMC Genom* 10: 242
35. Kawamura K, Shibata T, Saget O, Peel D, Bryant PJ (1999) A new family of growth factors produced by the fat body and active on *Drosophila* imaginal disc cells. *Development* 126: 211–219
36. Ringrose L, Rehmsmeier M, Dura J-M, Paro R (2003) Genome-wide prediction of Polycomb/Trithorax response elements in *Drosophila melanogaster*. *Dev Cell* 5: 759–771
37. Zimmerman SG, Merrihew GE, MacCoss MJ, Berg CA (2017) Proteomics analysis identifies orthologs of human chitinase-like proteins as inducers of tube morphogenesis defects in *Drosophila melanogaster*. *Genetics* 206: 973–984
38. Pesch Y-Y, Riedel D, Patil KR, Loch G, Behr M (2016) Chitinases and imaginal disc growth factors organize the extracellular matrix formation at barrier tissues in insects. *Sci Rep* 6: 18340
39. Broz V, Kucerova L, Rouhova L, Fleischmannova J, Strnad H, Bryant PJ, Zurovec M (2017) *Drosophila* imaginal disc growth factor 2 is a trophic factor involved in energy balance, detoxification, and innate immunity. *Sci Rep* 7: 43273
40. Kucerova L, Broz V, Arefin B, Maaroufi HO, Hurychova J, Strnad H, Zurovec M, Theopold U (2016) The *Drosophila* chitinase-like protein IDGF3 is involved in protection against nematodes and in wound healing. *J Innate Immun* 8: 199–210
41. Sawicka A, Seiser C (2012) Histone H3 phosphorylation – a versatile chromatin modification for different occasions. *Biochimie* 94: 2193–2201
42. Bellen HJ, Levis RW, He Y, Carlson JW, Evans-Holm M, Bae E, Kim J, Metaxakis A, Savakis C, Schulze KL et al (2011) The *Drosophila* gene disruption project: progress using transposons with distinctive site specificities. *Genetics* 188: 731–743
43. Krauchunas AR, Wolfner MF (2013) Molecular changes during egg activation. *Curr Top Dev Biol* 102: 267–292
44. Svoboda P, Franke V, Schultz RM (2015) Sculpting the transcriptome during the oocyte-to-embryo transition in mouse. *Curr Top Dev Biol* 113: 305–349
45. Lesch BJ, Dokshin GA, Young RA, McCarrey JR, Page DC (2013) A set of genes critical to development is epigenetically poised in mouse germ cells from fetal stages through completion of meiosis. *Proc Natl Acad Sci USA* 110: 16061–16066
46. Lesch BJ, Page DC (2014) Poised chromatin in the mammalian germ line. *Development* 141: 3619–3626
47. Dorighi KM, Swigut T, Henriques T, Bhanu NV, Scruggs BS, Nady N, Still CD, Garcia BA, Adelman K, Wysocka J (2017) Mll3 and Mll4 facilitate enhancer RNA synthesis and transcription from promoters independently of H3K4 monomethylation. *Mol Cell* 66: 568–576.e4
48. Local A, Huang H, Albuquerque CP, Singh N, Lee AY, Wang W, Wang C, Hsia JE, Shiau AK, Ge K et al (2018) Identification of H3K4me1-associated proteins at mammalian enhancers. *Nat Genet* 50: 73–82
49. Hörmanseder E, Simeone A, Allen GE, Bradshaw CR, Figlmüller M, Gurdon J, Jullien J (2017) H3K4 methylation-dependent memory of somatic cell identity inhibits reprogramming and development of nuclear transfer embryos. *Cell Stem Cell* 21: 135–143.e136
50. Bui WC (2002) Characterization and biological roles of oviduct-specific, oestrogen-dependent glycoprotein. *Reproduction* 123: 355–362
51. Gao Y, Liu X, Tang B, Li C, Kou Z, Li L, Liu W, Wu Y, Kou X, Li J et al (2017) Protein expression landscape of mouse embryos during pre-implantation development. *Cell Rep* 21: 3957–3969
52. Yang X, Zhao Y, Yang X, Kan FWK (2015) Recombinant hamster oviductin is biologically active and exerts positive effects on sperm functions and sperm-oocyte binding. *PLoS One* 10: e0123003
53. King RS, Anderson SH, Killian GJ (1994) Effect of bovine oviductal estrus-associated protein on the ability of sperm to capacitate and fertilize oocytes. *J Androl* 15: 468–478
54. Coy P, Cánovas S, Mondéjar I, Saavedra MD, Romar R, Grullón L, Matás C, Avilés M (2008) Oviduct-specific glycoprotein and heparin modulate sperm-zona pellucida interaction during fertilization and contribute to the control of polyspermy. *Proc Natl Acad Sci USA* 105: 15809–15814
55. Killian GJ (2004) Evidence for the role of oviduct secretions in sperm function, fertilization and embryo development. *Anim Reprod Sci* 82–83: 141–153
56. Hipfner DR, Cohen SM (1999) New growth factors for imaginal discs. *BioEssays* 21: 718–720
57. Martus NS, Verhage HG, Mavrogianis PA, Thibodeaux JK (1998) Enhancement of bovine oocyte fertilization *in vitro* with a bovine oviductal specific glycoprotein. *J Reprod Fertil* 113: 323–329

58. Kouba AJ, Abeydeera LR, Alvarez IM, Day BN, Buhi WC (2000) Effects of the porcine oviduct-specific glycoprotein on fertilization, polyspermy, and embryonic development *in vitro*. *Biol Reprod* 63: 242–250
59. Brand AH, Perrimon N (1993) Targeted gene expression as a means of altering cell fates and generating dominant phenotypes. *Development* 118: 401–415
60. Ni J-Q, Zhou R, Czech B, Liu L-P, Holderbaum L, Yang-Zhou D, Shim H-S, Tao R, Handler D, Karpowicz P et al (2011) A genome-scale shRNA resource for transgenic RNAi in *Drosophila*. *Nat Methods* 8: 405–407
61. Van Doren M, Williamson AL, Lehmann R (1998) Regulation of zygotic gene expression in *Drosophila* primordial germ cells. *Curr Biol* 8: 243–246
62. White-Cooper H (2012) Tissue, cell type and stage-specific ectopic gene expression and RNAi induction in the *Drosophila* testis. *Spermatogenesis* 2: 11–22
63. Chou TB, Perrimon N (1992) Use of a yeast site-specific recombinase to produce female germline chimeras in *Drosophila*. *Genetics* 131: 643–653
64. Prudêncio P, Guilgur L (2015) FLP/FRT induction of mitotic recombination in *Drosophila* germline. *Bio-Protocol* 5: e1458
65. Guilgur LG, Prudêncio P, Sobral D, Lizekova D, Rosa A, Martinho RG (2014) Requirement for highly efficient pre-mRNA splicing during *Drosophila* early embryonic development. *eLife* 3: e02181
66. Ribeiro AL, Silva RD, Foyn H, Tiago MN, Rathore OS, Arnesen T, Martinho RG (2016) Naa50/San-dependent N-terminal acetylation of Scc1 is potentially important for sister chromatid cohesion. *Sci Rep* 6: 39118
67. Gilliland WD, Hughes SF, Vietti DR, Hawley RS (2009) Congression of achiasmate chromosomes to the metaphase plate in *Drosophila melanogaster* oocytes. *Dev Biol* 325: 122–128
68. Livak KJ, Schmittgen TD (2001) Analysis of relative gene expression data using real-time quantitative PCR and the 2^{(-Delta Delta C(T))} Method. *Methods* 25: 402–408
69. Nelson JD, Denisenko O, Bomsztyk K (2006) Protocol for the fast chromatin immunoprecipitation (ChIP) method. *Nat Protoc* 1: 179–185
70. Kallio MA, Tuimala JT, Hupponen T, Klemelä P, Gentile M, Scheinin I, Koski M, Käksi J, Korpelainen EI (2011) Chipster: user-friendly analysis software for microarray and other high-throughput data. *BMC Genom* 12: 507
71. Smyth GK (2004) Linear models and empirical Bayes methods for assessing differential expression in microarray experiments. *Stat Appl Genet Mol Biol* 3: 1–25
72. Tripathi S, Pohl MO, Zhou Y, Rodriguez-Frandsen A, Wang G, Stein DA, Moulton HM, DeJesus P, Che J, Mulder LCF et al (2015) Meta- and orthogonal integration of influenza 'OMICS' data defines a role for UBR4 in virus budding. *Cell Host Microbe* 18: 723–735
73. Edgar R, Domrachev M, Lash AE (2002) Gene expression omnibus: NCBI gene expression and hybridization array data repository. *Nucleic Acids Res* 30: 207–210
74. King RC (1970) *Ovarian development in Drosophila melanogaster*. Amsterdam, The Netherlands: Academic Press